Vibrational Microspectroscopic Imaging: Spatial Resolution Enhancement

Sebastian Schlücker, Scott W. Huffman, Ira W. Levin

Laboratory of Chemical Physics, National Instiute of Diabetes, Digestive and Kidney Diseases, National Institutes of Health, Bethesda, MD 20892, USA

ABSTRACT

We propose a methodology for enhancing the diffraction limited spatial resolution attained in Raman and Fourier transform infrared microspectroscopic imaging techniques. Near-field scanning optical microscopy (SNOM) and spectroscopy employ apertureless and aperture approaches to provide ultra-high spatially resolved images at the nanometer level. In contrast, we employ conventional spectral acquisition schemes modified by spatial oversampling with the subsequent application of deconvolution techniques. As an example, this methodology is applied to flat samples using point illumination. Simulated data, assuming idealized sample concentration profiles, are presented together with experimental Raman microspectroscopic data from chemically and morphologically well-defined test samples. Intensity profiles determined using conventional mapping and imaging techniques are compared to those obtained by the probe/deconvolution methodology.

Keywords: Vibrational microspectroscopic imaging, Raman and infrared spectroscopy, spatial resolution, spatial oversampling, deconvolution techniques

1. INTRODUCTION

Raman and infrared microspectroscopic imaging techniques provide contrast based on the intrinsic molecular properties of the sample, obviating the requirement of external stains or molecular labels. Common methods for acquiring spatially resolved Raman data are based on point, line and global imaging approaches.[1–3] Fourier Transform infrared (FT IR) microspectroscopic imaging acquires simultaneously thousands of spectra by coupling a focal plane array (FPA) detector to a Michelson interferometer.[4,5] The maximum spatial resolution attainable in conventional microscopy is given by the Abbé diffraction limit. Scanning near-field optical microscopy (SNOM) and spectroscopy, however, are capable of providing chemical information on a nanometer-scale.[6] In contrast to SNOM spectroscopic methods, we propose an alternative approach for obtaining ultra-high spatially resolved images using conventional techniques employed in both Raman and infrared microspectroscopic mapping and imaging procedures. In combination with spatial oversampling and the subsequent application of deconvolution techniques, spectral intensities reflecting actual sample concentrations are determined as a function of spatial coordinates.

2. THEORY

From the principles of Fourier optics, the observed intensity profile $h(X)$ for Raman mapping experiments arises from the convolution ($\otimes$) of the laser beam $f(X-x)$ probing the actual or true sample concentration profile $g(x)$:

$$h(X) = f(X-x) \otimes g(x), \tag{1}$$

Further author information: (Send correspondence to I.W.L.)
I.W.L.: E-mail: iwl@helix.nih.gov, Telephone: 1 301 496 6844; Fax: 1 301 496 0825

Biomedical Vibrational Spectroscopy/Biohazard Detection Technologies, edited by
A. Mahadevan-Jansen, M. G. Sowa, G. J. Puppels, Z. Gryczynski, T. Vo-Dinh, J. R. Lakowicz,
Proc. of SPIE Vol. 5321 (SPIE, Bellingham, WA, 2004) · 1605-7422/04/$15 · doi: 10.1117/12.528652

or:

$$h(X) = \int_{-\infty}^{\infty} f(X - x)\, g(x)\, dX, \tag{2}$$

where X and x are spatial coordinates.

This concept is illustrated in Figure 1 for a Gaussian-shaped laser beam where the concentration profile of the sample along the spatial coordinate X is represented by a rectangular or boxcar function. Raster scanning is achieved by either shifting the sample on a motorized stage or by scanning the laser beam across the sample by a set of mirrors. The profile of the laser beam is delineated, as an example, for five discrete positions, x_1 to x_5. At positions x_1 and x_5, where no sample is present, the detected intensity is zero. The maximum intensity is observed for positions around x_3. When the laser beam is centered at x_2 and x_4, the edges of the boxcar profile $g(x)$, only the half maximum intensity is detected. In this model, the differences between the actual and the detected intensity profiles, $g(x)$ and $h(X)$, respectively, arise from sample intensity contributions at $\pm\, \Delta x_i$ when the laser beam is centered at x_i. This description does not explicitly include additional optical properties, such as scattering effects at the edges of the sample.

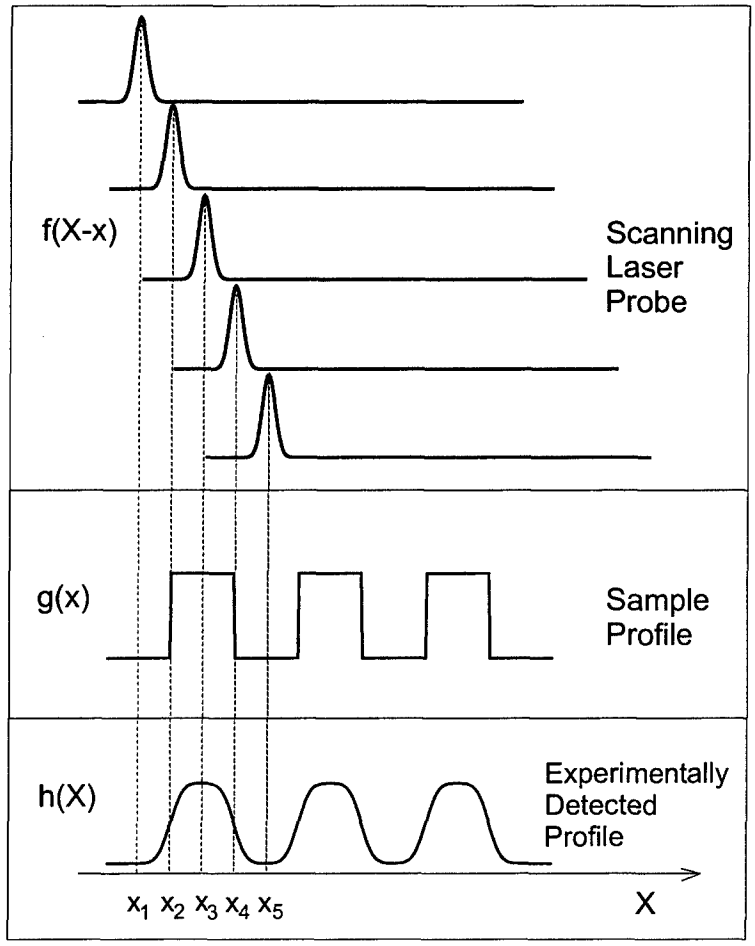

Figure 1. Illustration of the scanning probe/deconvolution approach in Raman microspectroscopic mapping.

In raster scanning, the detected profile **h** is calculated simply for a finite number of steps by the matrix multiplication of **F**, which contains the probe profiles at each sampling position, with the concentration profile **g**:

$$\mathbf{h} = \mathbf{F}\,\mathbf{g}, \tag{3}$$

or

$$\mathbf{g} = \mathbf{F}^{-1}\,\mathbf{h}. \tag{4}$$

For Fourier Transform Infrared (FT IR) microspectroscopic imaging data acquired in a transmission mode, the same formalism is applied. In contrast to Raman point mapping experiments, in which a Gaussian-shaped laser beam probes the sample, the grid of pixels of a focal plane array (FPA) detector acts as an aperture in the infrared imaging experiments. In Figure 2, the aperture **F** consists of seven FPA pixels, while the sample profile **g** is assumed to be a boxcar function. In this case, triangular intensity profiles **h** are detected. In Figure 2, both aperture and detected intensity profiles are shown, as an example, for three measurements employing spatial oversampling; the sample concentration is probed at spatial intervals which are small compared to the dimensions of an individual FPA pixel. For the first three of the seven FPA pixels, the correlation between individual pixels and the corresponding detected intensity values is indicated by dashed lines.

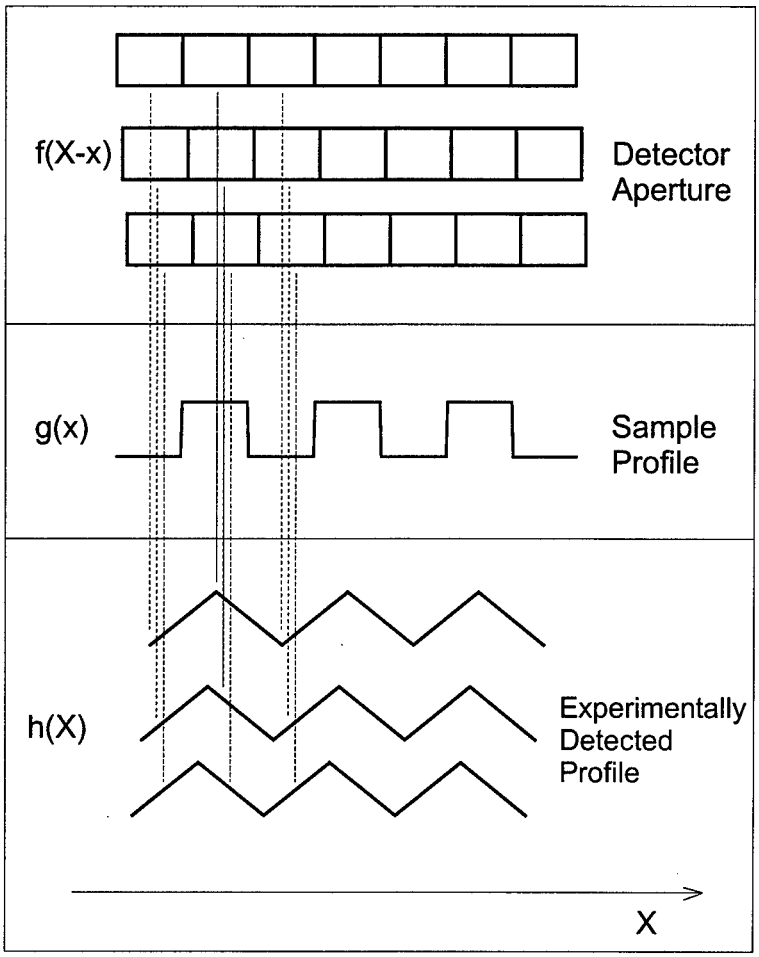

Figure 2. Illustration of the aperture scanning/deconvolution approach in FT IR microspectroscopic imaging employing spatial oversampling.

The implications of this approach are as follows: First, it allows a comparison between experimentally detected and theoretically predicted intensity profiles for either probe laser or aperture functions and known sample concentration profiles (Equation 3). Second, and more importantly, the model allows the possibility of extracting the true intensity profile by deconvolution procedures using the experimentally determined profile of the probe beam or aperture function (Equation 4). This strategy has, in combination with spatial oversampling, the potential of generating chemical images at resolutions greater than the diffraction limit.

3. EXPERIMENTAL

Raman microspectroscopic experiments were carried out on a Raman imaging system consisting of a dispersive spectrometer (Renishaw, Model Ramascope System 2000) coupled to a microscope (Leica, Model DM-LM). Raman excitation was provided by the 514.5 nm line of an argon ion laser (Spectra Physics, Model 2014). The laser radiation was focused on the sample by an infinity-corrected × 50 objective (Leica, Model N Plan, NA = 0.75). The backscattered light was passed through a set of holographic notch filters (Kaiser Optical Systems) and focused on the entrance slit of a single-stage monochromator (25 cm focal length, grating with 1800 grooves/mm). A slit width corresponding to a resolution of 4 cm^{-1} at 520 cm^{-1} was employed. Raman data were recorded with a thermoelectrically cooled CCD (Renishaw, Model RenCam, pixel size 22 × 22 μm^2). Experiments were performed on a scanning electron microscopy (SEM) standard target containing 5-μm squares of silicon (Ladd Research Industries, Model 53130 SEM). For point mapping experiments, the sample was shifted on a motorized stage (Renishaw, Model RGH22) using the vendor-supplied software (Renishaw, WiRe 1.3).

4. RESULTS AND DISCUSSION

Raman point mapping

A bright-field microscope image of the SEM target is shown in Figure 3A. The bright areas represent aluminum, the underlying dark silicon squares appear bright.

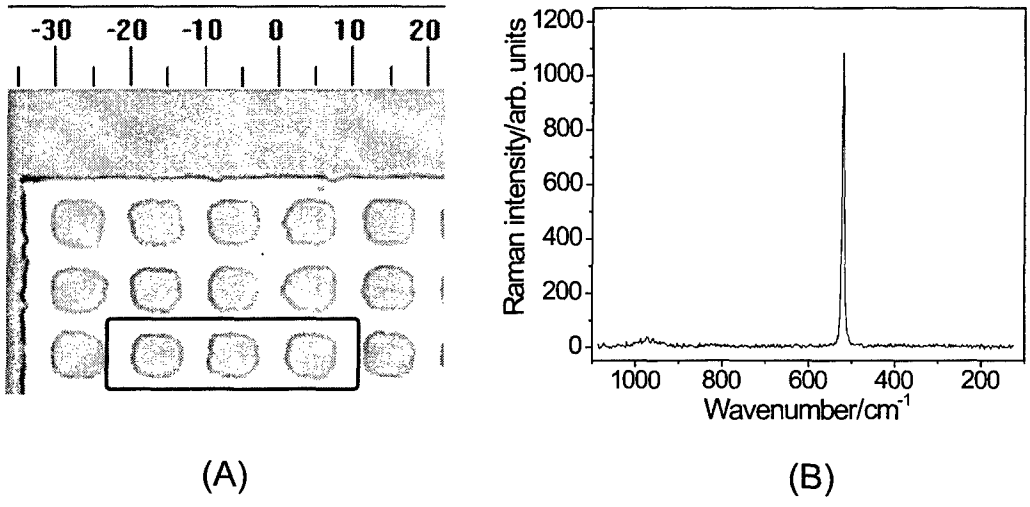

Figure 3. (A) Bright-field image of the silicon/aluminum test sample. Raman images of the region delineated by solid lines are shown in Figure 4; (B) Raman spectrum of silicon.

In contrast to conventional light microscopy, which is solely based on the material's reflectivity, Raman spectroscopy allows the chemical identification based on intrinsic vibrational spectroscopic signatures. The Raman spectrum in Figure 3B exhibits the strong and characteristic first-order phonon band of silicon at 520 cm^{-1}. Intensity values at this wavenumber position are used to generate intensity profiles and chemical images of silicon from both the Raman mapping and global imaging experiments.

Figure 4 displays images and horizontal intensity profiles for the region delineated by the solid lines in Figure 3A. Figure 4A shows the bright-field image with an inverted contrast. The Raman images shown in Figures 4b and C were obtained with wide-field illumination (direct imaging, B) or reconstructed from point mapping data (raster scanning, C). The images and intensity profiles in Figures 4A and B indicate edges of the silicon squares, which represent artifacts remaining after the etching process of the target. In contrast to the intensity profiles in Figures 4A and B, which both correspond to images obtained with wide-field illumination, the raster scanned, Raman intensity profile in Figure 4C fails to resolve these edges.

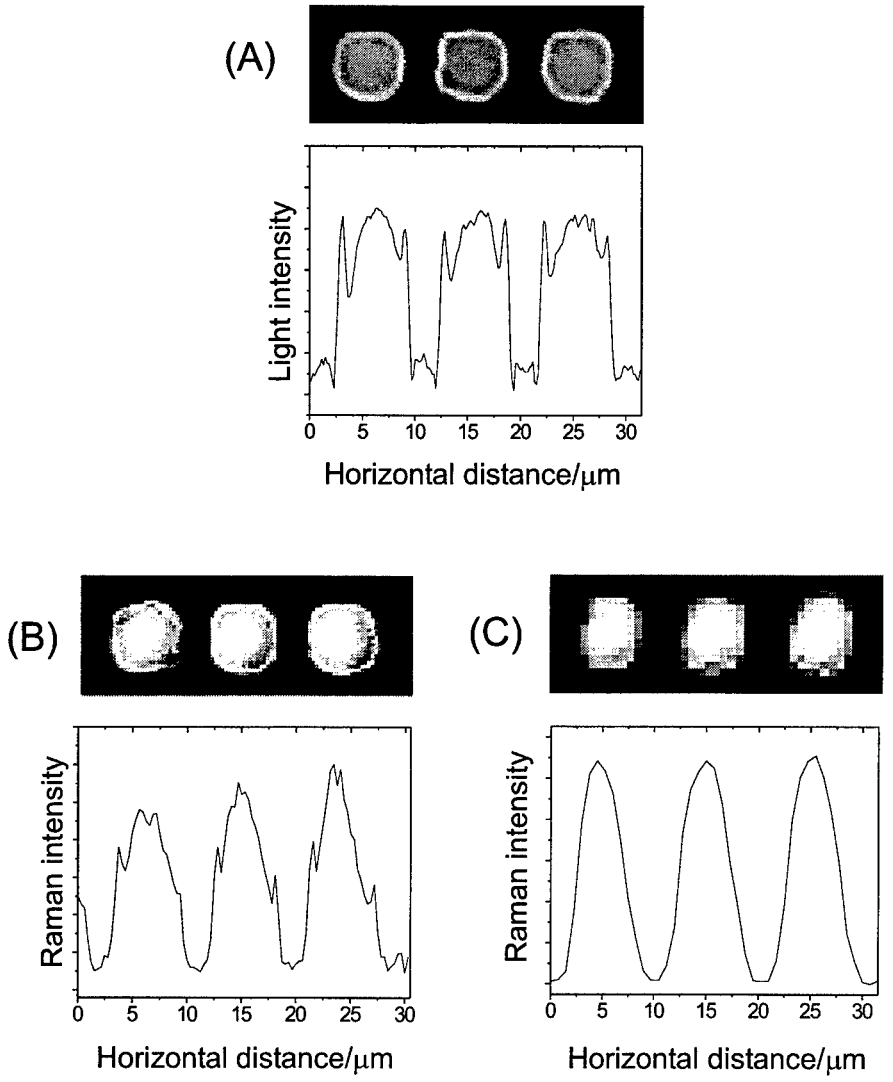

Figure 4. Images and horizontal intensity profiles of the region delineated by solid lines in Figure 3: (A) Bright-field image with inverted contrast; (B) Global Raman image; (C) Raman image reconstructed from point mapping data.

From Equation (4), an estimate of the true concentration profile **g** is calculated when both the detected intensities **h** and the laser beam profile entering **F** are known functions. Figure 5A shows the experimentally determined laser profile (hollow circles) and a fitted Gaussian profile (solid line, line width 0.5 μm). The experimentally observed intensities **h** shown in Figure 5C are the same as in Figure 4C. The true sample concentration profile **g** was calculated using Equation (4). In this case, the probe matrix contains integrated intensities based on the areas covered by a 1.0 μm diameter Gaussian beam displaced by 0.75 μm intervals. This corresponds to an example of spatial oversampling. The narrower average full width of half maximum (FWHM) of 4.8 μm for the true profile compared with 5.0 μm for the detected profile indicates a successful spatial deconvolution. The true profile, **g**, using data acquired at 0.75 μm intervals, recovers the basic features observed in the global Raman image at an experimental spatial resolution of 0.3 μm (Figure 4B).

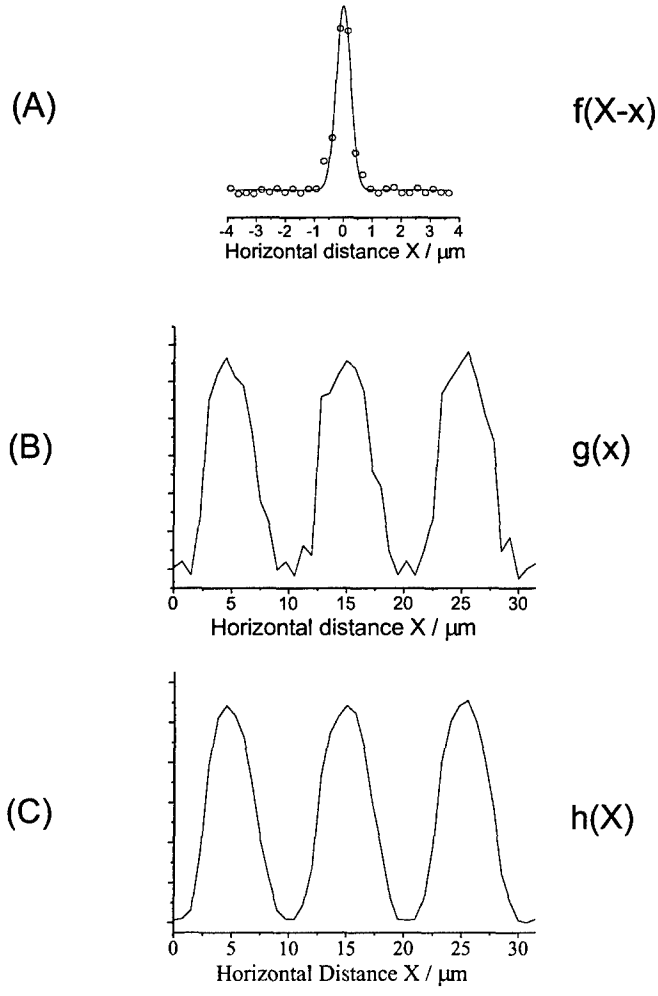

Figure 5. (A) Experimentally determined laser probe profile (hollow circles) and a fitted Gaussian profile (solid line, 0.5 μm width); (B) Calculated true or actual sample concentration profile; (C) Experimentally observed intensity profile (Raman point mapping).

5. CONCLUSIONS

Our proposed methodology has the potential of generating chemical images at high spatial resolutions beyond the diffraction limit. In order to demonstrate the limits of the technique, further experiments involving spatial oversampling in combination with deconvolution techniques, are envisioned on a variety of chemical and biological samples. In particular for FT IR imaging, the challenge is to obtain spatial resolutions at the sub-micron level for applications in imaging characteristics of cellular organelles.

ACKNOWLEDGMENTS

S.S. acknowledges financial support from the German Science Foundation (DFG-Forschungsstipendium).

REFERENCES

1. G. Turrell, J. Corset, *Raman Microscopy*, Academic Press: San Diego, 1996.
2. P. J. Treado, M. P. Nelson, *"Raman Imaging"* in: *Handbook of Vibrational Spectroscopy*, J. M. Chalmers, P. R. Griffiths (Eds.), Vol. 2, Wiley, 2002.
3. S. Schlücker, M. D. Schaeberle, S. W. Huffman, I. W. Levin, *Anal. Chem.*, **75**, 4312 - 4318, 2003 .
4. E. N. Lewis, P. J. Treado, R. C. Reeder, G. M. Story, A. E. Dowrey, C. Marcott, I. W. Levin, *Anal. Chem.*, **67**, 3377 - 3381, 1995.
5. R. Bhargava, I. W. Levin, *Trends in Appl. Spectrosc.*, **3**, 57 - 71, 2001.
6. R. Zenobi, V. Deckert, *Angew. Chem. Int. Ed.*, **39**, 1746 - 1756, 2000.